WEST-EAST HIGH SPEED FLOW FIELD CONFERENCE
19-22, November 2007
Moscow, Russia

INVESTIGATION OF HEAT TRANSFER OVER THE GENERIC MODEL OF MARTIAN DESCENT VEHICLE

V. Borovoy[*] I. Egorov[*] P. Omaly[**] O. Rouzand[***] and A. Skuratov[*]

**Central Aerohydrodynamic Institute (TsAGI)*
Zhukovsky st. 1, Zhukovsky, Moscow region, 140180, Russia
Email: Skuratov@progtech.ru, Volf_Borovoy@m9com.ru
***CNES, 18, avenue Edouard Belin, 31401 Toulouse Cedex 4, France*
**** ONERA, 2, avenue Edouard Belin, 31055 Toulouse Cedex 4, France*

Key words: generic model, Martian descent vehicle, base region, separation flow, heat flux, numerical simulation.

Abstract. The purpose of this paper is to investigate convective heat flux distribution over the Generic model of Martian descent vehicle. The main attention has been paid to heat transfer investigation in the model base region where heat fluxes are rather small. High sensitive heat flux sensors were used. The model has been installed on a side strut. It gives possibility to investigate heat transfer in the model base region including vicinity of the rear stagnation point. Experiments have been performed in two short duration wind tunnels at Mach numbers M_∞=7.9, 12 and 20.4 in air, carbon dioxide and nitrogen respectively. The tests were accompanied by numerical simulations of laminar flow. Experiments have shown that heat flux in the base region is around 1−2.5% of the front stagnation-point heat flux. Numerical heat flux values are in concord with the data except for vicinity of the rear stagnation point.

1. INTRODUCTION

The main goal of future Martian missions will be delivery of the Martian soil specimen to the Earth. Martian Descent Vehicle payload at Martian atmosphere entry is supposed to be placed in the afterbody region. If the payload container has no heat protection, excess of the real heat flux over the predicted one can result in damage of the payload. If the payload has a heat shield, its weight can constitute a significant part of the total heat protection weight. Therefore, rather accurate estimation of the convective and radiation base heat flux is necessary in both cases.

One meets at least two significant difficulties at experimental investigations of the heat transfer in the base region. The first one is connected with low level of heat flux and necessity of high sensors sensibility. The second one is caused by influence of support device on the flow and heat transfer in the base region. Now the base stings are usually used, see for example[1]. At that, measurements of heat flux at the rear stagnation point are impossible because this point is occupied by the sting. The base sting disturbs flow and heat transfer in the whole base region. Therefore, a side strut is used in this study.

Experiments were supported by numerical simulations. The laminar flow is numerically simulated by solving of the 2D system of Navier-Stokes equations.

2. MODEL. DATA PROCESSING

The generic model of Martian descending vehicle corresponding to the test-case TC3 configuration of the European Work Group[2] was under consideration, Figure 1. Full scale scheme of the vehicle is indicated left (dimensions are in cm). The investigated model has diameter D=120 mm (see photo in Figure 1 right). Its payload container represents itself a cylinder. The model has been installed in the wind tunnels on the side strut which allows investigating heat transfer in the base region. The model was equipped with 61 heat flux sensors developed at TsAGI. On the frontal model surface, sensors "thin wall" were used, and high sensitive foil thermocouple sensors were installed on the base surface. Method of heat sensors data processing is described in[3]. Pressure has been measured at six points by the "Kulite" sensors presented by CNES.

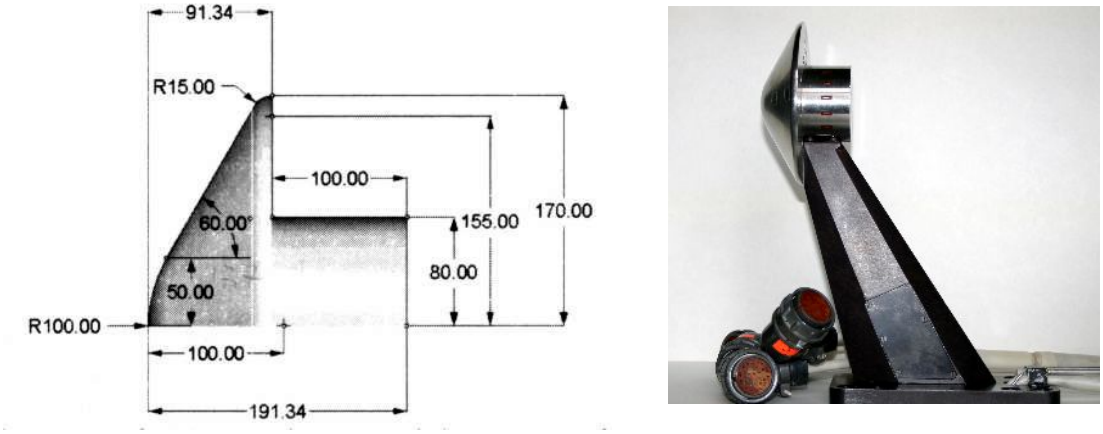

Figure 1. Generic model

3. TEST REGIMES

Experiments have been performed in two TsAGI's short duration wind tunnels:

1) In Shock wind tunnel UT-1 which operated as a Ludwieg tunnel at Mach number $M_\infty = 7.9$ in air. Total pressure is $P_t \approx 10$ bar, total temperature is $T_t \approx 750$K. The corresponding Reynolds number is $Re_{\infty, D} \approx 2.57\times10^5$ (D=120 mm is the model diameter). A profiled nozzle with exit diameter D_{exit}=500 mm was used.
2) In Hot Shot wind tunnel IT-2 at M_∞ =12 (in carbon dioxide) and at M_∞ =20.4 (in nitrogen). The total parameters are as following:

Nitrogen: P_t=546 bar, T_t=1960K. Corresponding Reynolds number is $Re_{\infty, D}=1.79\times10^5$.

Carbon dioxide: P_t=317 bar, T_t=1670K. Corresponding Reynolds number is $Re_{\infty, D}=0.41\times10^5$.

A conical nozzle with exit diameter D_{exit}=526 mm was used in IT-2.

In all the test cases, the gas can be considered as a perfect one with a constant specific heat ratio γ. It was assumed for air and nitrogen γ=1.4, and for carbon dioxide γ=1.26. The last value was determined by measurement of bow wave stand off ahead of blunt body.

Before this test campaign, measurements of stagnation pressure and heat flux distributions in test sections of both wind tunnels were performed. Pitot and heat flux rakes with 27 orifices were used for this purpose. It allows us to determine dimensions of dynamic and heat cores at the section where the model was situated (see the Table 1). Besides mean values of Mach number M_a in the dynamic core are indicated in the Table 1, too.

Wind tunnel	Gas	M_a	D_d, mm	D_h, mm	D_d/D_{exit}	D_h/D_{exit}
UT-1	Air	7.89	320	240	0.64	0.48
IT-2	Carbon dioxide	12.02	240	200	0.46	0.38
	Nitrogen	20.41	200	240	0.38	0.46

Table 1. Dynamic and heat cores dimensions in wind tunnels test sections

It is visible from the Table that model with diameter D=120 mm is located completely inside the dynamic and heat cores of both wind tunnels.

4. TEST RESULTS

Shadow photograph of the flow around the model taken during one of the test runs in the UT-1 wind tunnel is shown in Figure 2.

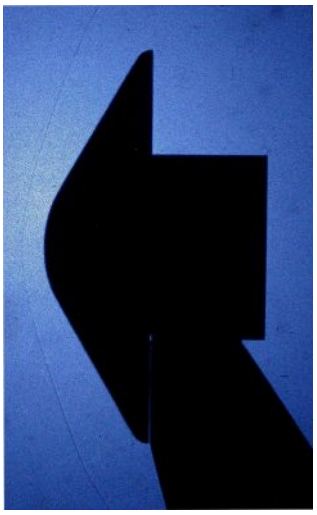

Figure 2. Shadow picture of the model overflow. UT-1. Air flow. M_∞=7.9

Because of the low gas density, features of flow can be detected only in the bow shock wave region. To determine the flowfield in the base region, we use numerical results presented in Figure 3 (CFD from here).

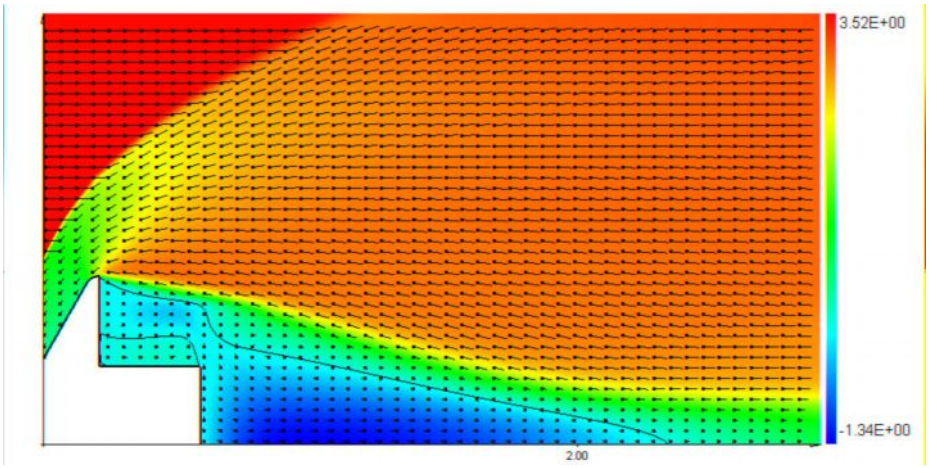

Figure 3. CFD. Longitudinal velocity field with isolines U=0 and vector diagram

Numerical simulation has been performed for the experimental flow conditions. In the picture, field of longitudinal velocity U is shown. Besides, the vector diagram and isolines U=0 are presented. The whole base region is occupied by a global separation zone which starts practically at the model shoulder. It's visible that the flow separated near the shoulder doesn't reattach to the cylinder surface due to its small length and diameter. Thus, one may believe that no heat flux peak will appear on the cylinder generatrix. Isoline U=0 enables to determine coordinate of the near-wake closure point.

Flow patterns calculated for the nitrogen and carbon dioxide flows in IT-2 are similar to the air flow in UT-1.

Heat flux distribution along the model heatshield for nitrogen flow at M_∞=20.4 is shown in Figure 4. As a whole, heat flux distribution corresponds to the flow pattern around a body type sphere-cone. CFD heat flux distribution for laminar flow is depicted here, too. It's possible to mark satisfactory coincidence between experimental and CFD data.

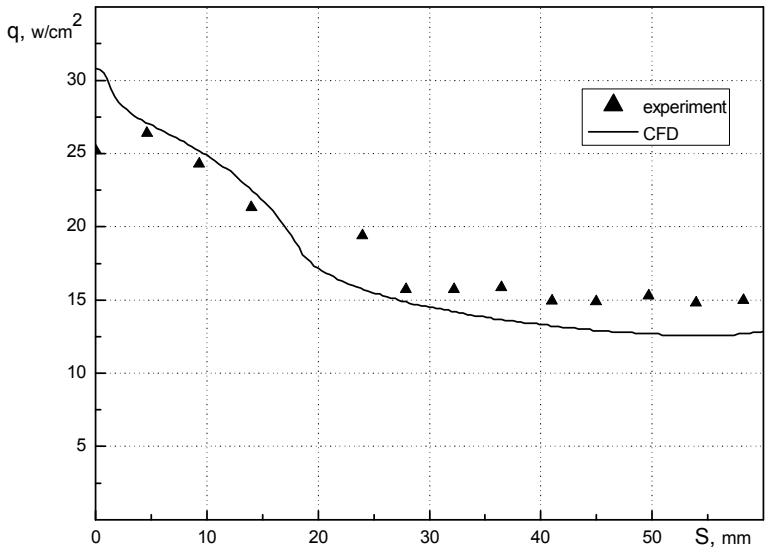

Figure 4. Heat flux distribution along heatshield surface. IT-2. Nitrogen flow. M_∞=20.4

Comparison of relative heat flux data on the heatshield surface obtained in both wind tunnels is made in Figure 5 (S=0 is the coordinate of the forward stagnation point, q_s is the measured heat flux at the forward stagnation point). Of course, it should be taken into account that the tests have been performed with different gases and at different flow parameters (Mach and Reynolds numbers). Nevertheless, the comparison can appear useful because the flow over the model at all conditions studied has some common features: 1) Mach numbers in all cases are hypersonic, 2) all tests have been performed at comparable Reynolds numbers (about 10^5, based on the model diameter), that guarantees laminar flow over the front surface and in the wake. In addition, according to the numerical simulation, flow pictures in the base region are similar in all cases.

Relative heat flux values practically coincide in the range of S=±20 mm, i.e. on the spherical part and at the beginning of the conical part. On the conical part (at S>20 mm), the relative data for carbon dioxide and nitrogen flows in IT-2 wind tunnel are close to each other, and the data for air flow in UT-1 wind tunnel are somewhat lower. The reason may be owing to the difference in the Mach numbers.

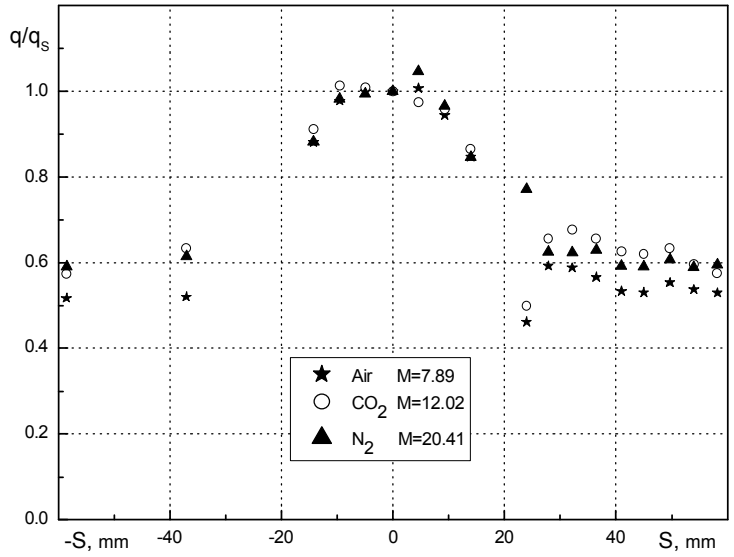

Figure 5. Relative heat flux distribution on the heatshield surface for all test regimes

Relative heat flux distribution q/q_s in the model base region is submitted in Figure 6. Different parts of the model surface are marked in the graph, namely: base surface of heatshield, cylindrical surface of container and cylinder butt-end. The rear stagnation point has coordinate S=165.1 mm. Calculated values of relative heat flux are depicted, too. Pay attention to low heat flux levels: on the heatshield base surface and cylinder generatrix, heat flux is less than 0.1% of heat flux at the forward stagnation point. Only at the rear stagnation point heat flux reaches 1.4%. Taking into account complicated flow character in the base region, it may be assumed that CFD and experimental relative heat fluxes concord satisfactory on the base heatshield surface and on the cylinder generatrix. Only on the butt-end of the cylinder CFD heat flux exceeds the experimental one several times.

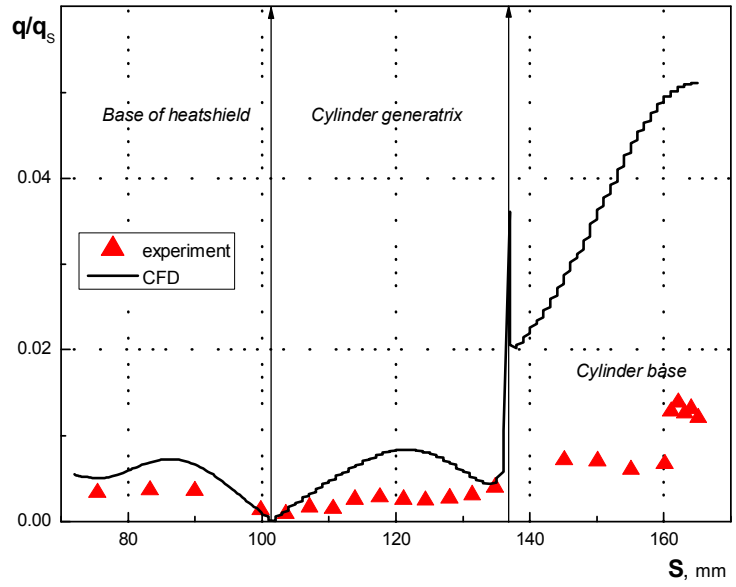

Figure 6. Relative heat flux distribution in the base region. IT-2. Nitrogen flow. M_∞=20.4

Relative heat flux distributions in the base region for all the test regimes are presented in Figure 7. One can see that relative heat fluxes for nitrogen and carbon dioxide flows are practically coincident, whereas heat flux for air flow is rather larger.

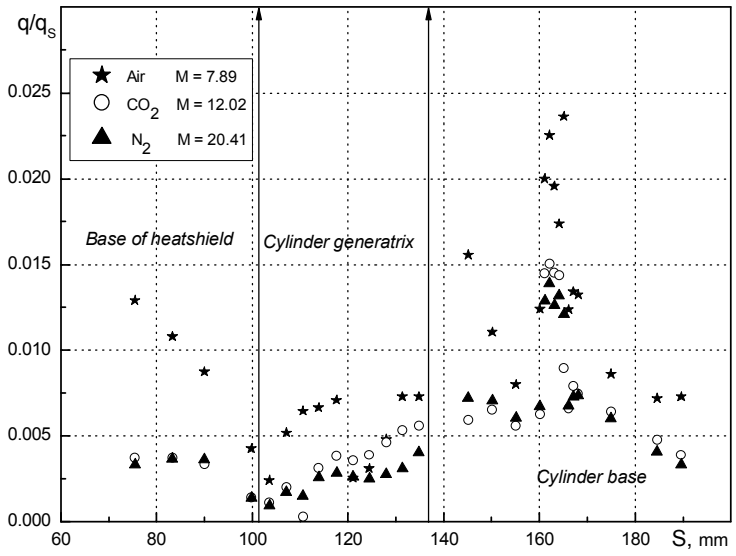

Figure 7. Relative heat flux distribution in the model base region for all test regimes

Because the Reynolds numbers being comparable for all test regimes (around 10^5), it is possible that the main parameter influencing on heat flux in the base region is again the Mach number. If it is so, one can conclude that the higher is the Mach number, the lower is the relative heat flux.

It is known that at Mach numbers $M \geq 5$, distribution of normalized heat flux over front surface of a blunt body does not depend on Mach number (hypersonic stabilization. Distribution of relative heat flux on the model heatshield confirms it, Figure 5). It seems

that for a body like the one studied, stabilization of the heat flux distribution in the base region starts at Mach number approximately 12.

Heat flux values at the forward stagnation point and maximal heat flux values in the vicinity of the rear stagnation point are given in Table 2. Relative values of heat flux q_{max}/q_s at the model base region are given too.

Reduced maximal values of the heat flux on the cylinder butt-end in nitrogen and carbon dioxide are close, around 1.5%. In the air flow, this value is 60% higher, around 2.4%.

Gas	M_∞	Forward stagnation point, q_s [W/cm^2]	Maximal value in the cylinder base region, q_{max} [W/cm^2]	q_{max}/q_s
Air	7.9	5.39	0.13	0.024
Nitrogen	20.4	25.18	0.35	0.014
Carbon dioxide	12.0	18.64	0.28	0.015

Table 2. Heat flux at the forward and rear stagnation points

It is interesting to compare the presented above results with the data obtained in the base region of another model of Martian descent vehicle (MDV)[4] shown in Figure 8.

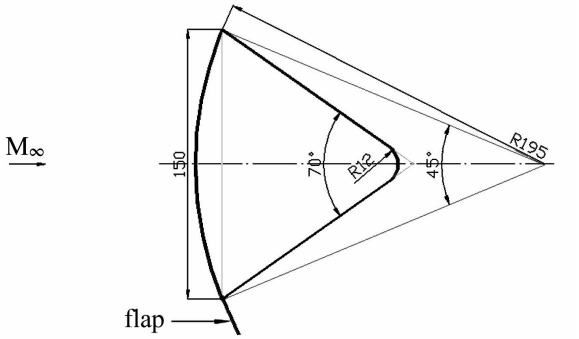

Figure 8. Model of Martian descent vehicle (MDV)

The main difference between the models concerns the shape of the pay load container: the container shown in Figure 1 is situated deeper in the separated region than the one shown in Figure 8; in addition the first container has a flat butt-end in contrast to the second one shaped as a sphere with small radius. It results in significant lower heat flux values in the first case (compare Figure 6 with Figure 9). We expect that this advantage of the new shape will be kept at angles of attack. The coming tests should answer on his question.

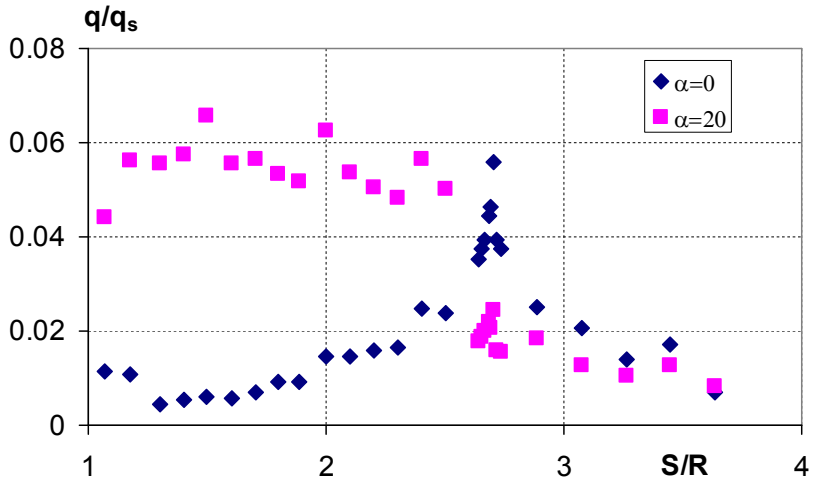

Figure 9. Relative heat flux distribution in the base region of MDV model. IT-2 [3]. Nitrogen flow. M_∞=20.4

Pressure distribution along the model generatrix is submitted in Figure 10 for nitrogen flow at M_∞=20.4 in IT-2 wind tunnel. The first two points are situated on the frontal surface of heatshield and the last point – at the vicinity of the rear stagnation point. At the forward stagnation point (S=0) measurement was not performed because this point is occupated by the heat flux sensor. Instead the calculated value of stagnation pressure is indicated at this point ("gasdynamics" in the legend). CFD pressure distribution is plotted, too

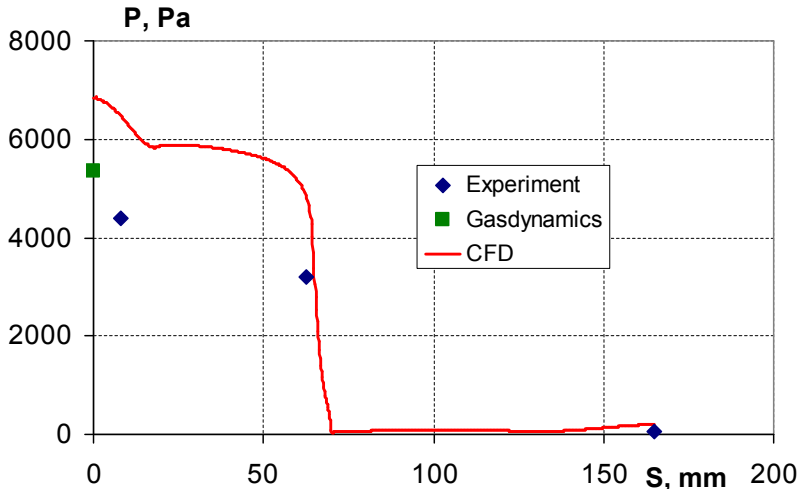

Figure 10. Experimental and CFD pressure distributions. IT-2. Nitrogen flow

CFD pressure distribution is systematically higher than the experimental one though the behavior of the calculated distribution completely reproduces the experimental one.

Comparison of the pressure values at all the test regimes is shown in Figure 11. In Table 3 experimental pressure values are indicated. At the forward stagnation point, the calculated pressure behind the normal shock P_s is specified. Maximal value of the relative pressure value P_{max}/P_s=1.34% in the base region takes place in carbon dioxide flow, the minimal one 0.97% is found in the air flow.

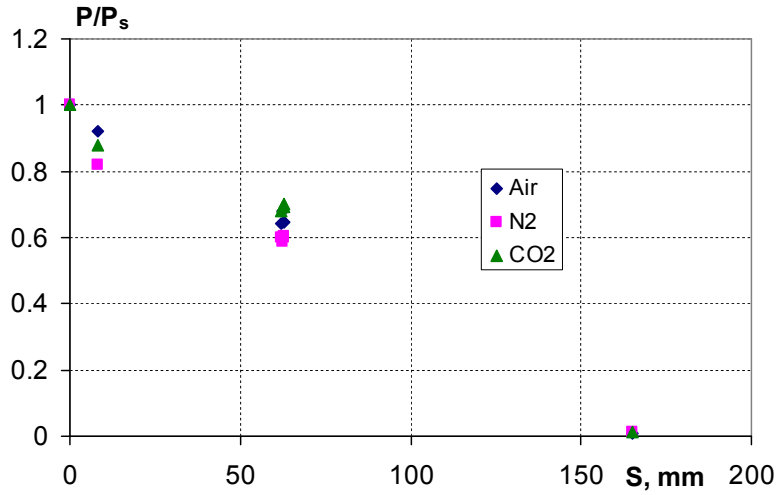

Figure 11. Relative pressure distribution for all test regimes

Gas	M_∞	Forward stagnation point, calculated P_s [Pa]	Maximal value in the cylinder base region P_{max} [Pa]	P_{max}/P_s
Air	7.9	9510	92	0.0097
Nitrogen	20.4	5343	66	0.0123
Carbon dioxide	12.0	2855	38	0.0134

Table 3. Pressure values on the model surface

CONCLUSION

1. Experimental investigation of the flow around the Generic Model of Martian descent vehicle has been performed in two wind tunnels TsAGI: UT-1 wind tunnel (test gas is air) and IT-2 wind tunnel (nitrogen and carbon dioxide). Heat flux has been measured in 61 points and pressure in 6 points.

A data bank has been created, which contains information about heat exchange over the Generic Model streamlined by an approximately perfect gas. Especially detailed information is presented for heat transfer on the base surfaces (back surface of the heat shield, side surface of the cylindrical payload-container, and base surface of the container).

2. Over most of the base region, the heat flux is rather low and comes to about 1% of the heat flux value at the forward stagnation point.

Due to the small dimensions of the payload container, the global separation flow generated behind the heatshield doesn't reattach to the cylindrical surface of the container. Therefore no heat peak is created on the cylindrical surface. Only small heat transfer augmentation can happen on the cylinder due to presence of secondary vortices.

3. At the vicinity of the rear stagnation point, the relative heat flux is about 2.4% in UT-1 wind tunnel (Mach number M=8, air flow) and 1.5% in IT-2 wind tunnel (M=12, carbon dioxide flow and M=20, nitrogen flow).

4. Pressure on the cylinder butt-end is equal to 1% of stagnation pressure behind the normal shock in UT-1 wind tunnel and approximately 1.2% in IT-2 wind tunnel.

5. The CFD results for heat flux distribution are in accordance with the experimental data for all the model surfaces except for the cylinder butt-end where the calculated values are several times higher than the experimental data.

This work was performed under support of INTAS (Project No. 03-51-5204) and Russian Foundation for Basic Researches (Project No. 05-01-00562a).

REFERENCES

[1] T. Horvath, N. Heiner, M. Olguin, F. Cheatwood, and P. Gnoffo. "Afterbody heating characteristics of a proposed Mars sample return orbiter". *AIAA Paper 2001-3068*, 15 p. (2001).

[2] J.M. Charbonnier, J. Couzi, W. Dieudonne, J-L Verant. Workshop 2003 Radiation of High Temperature Gas; TC3: Definition of an axially symmetric testcase for high temperature gas radiation prediction in Mars atmosphere entry. *NG104-07-TF-001-CNES.* May 15th (2003).

[3] V. Borovoy, S. Boldyrev, I. Egorov, A. Korolev, A, Skuratov, A. Tarantin, Yu. Zhilin. "Methodology of heat transfer investigation around a Martian vehicle in a short duration wind tunnel". *Proceedings of the 4th European Symp. on Aerothermodynamics for Space Vehicles.* Capua, Italy, 15-18 October 2001, Pp. 225-232 (2001).

[4] V. Borovoy, I. Egorov, A. Skuratov, and I. Struminskaya. "Convective heat transfer investigation on the typical models of the Martian descent vehicle" *Proceedings of the Second European Conference for Aerospace Sciences.* 1−6 July, 2007, Brussels, Belgium. http://www.vki.ac.be/eucass2007 restricted